M-shaped Grating by Nanoimprinting: A Replicable, Large-Area, Highly Active Plasmonic Surface-Enhanced Raman Scattering Substrate with Nanogaps

Zhendong Zhu, Benfeng Bai,* Huigao Duan, Haosu Zhang, Mingqian Zhang, Oubo You, Qunqing Li,* Qiaofeng Tan, Jia Wang, Shoushan Fan, and Guofan Jin

Plasmonic nanostructures separated by nanogaps enable strong electromagnetic-field confinement on the nanoscale for enhancing light-matter interactions, which are in great demand in many applications such as surface-enhanced Raman scattering (SERS). A simple M-shaped nanograting with narrow V-shaped grooves is proposed. Both theoretical and experimental studies reveal that the electromagnetic field on the surface of the M grating can be pronouncedly enhanced over that of a grating without such grooves, due to field localization in the nanogaps formed by the narrow V grooves. A technique based on room-temperature nanoimprinting lithography and anisotropic reactive-ion etching is developed to fabricate this device, which is cost-effective, reliable, and suitable for fabricating large-area nanostructures. As a demonstration of the potential application of this device, the M grating is used as a SERS substrate for probing Rhodamine 6G molecules. Experimentally, an average SERS enhancement factor as high as 5×10^8 has been achieved, which verifies the greatly enhanced light–matter interaction on the surface of the M grating over that of traditional SERS surfaces.

Z. Zhu, Prof. B. Bai, H. Zhang, M. Zhang, O. You,
Prof. Q. Tan, Prof. J. Wang, Prof. G. Jin
State Key Laboratory of Precision Measurement
Technology and Instruments
Department of Precision Instrument
Tsinghua University
Beijing 100084, China
E-mail: baibenfeng@mail.tsinghua.edu.cn

Z. Zhu, Prof. Q. Li, Prof. S. Fan
Tsinghua-Foxconn Nanotechnology Research Center
Department of Physics
Tsinghua University
Beijing 100084, China
E-mail: qunqli@mail.tsinghua.edu.cn

Prof. H. Duan
Key Laboratory for Micro-Nano Optoelectronic Devices
of Ministry of Education
Hunan University
Changsha 410082, China

1. Introduction

Surface plasmons (SPs) are collective oscillations of free-electron-density gas on a metal surface, which can funnel the electromagnetic (EM) field into subdiffraction volumes and thus have various applications in modulating light–matter interactions on the nanometer scale.[1,2] This energy-focusing effect is particularly promising in metallic nanostructures with tiny gaps,[1,3] such as V grooves,[4] nanoslots,[5] and self-similar chains of metal nanoparticles,[6] due to the strong localization of SPs in the nanogaps. When the SPs are local-ized in a sub-diffraction-limited tiny volume such as a nano-particle[7] or nanocavity,[8] which is referred to as localized surface plasmons (LSPs),[9] the localized EM field may be greatly enhanced by orders of magnitude compared with the incident field (thus called the EM field "hot spot").[10] The LSPs can be further steered via the intercoupling of various LSP resonance modes in complex metallic nanostructures such as plasmonic nanoshells,[11] nanodimers,[5] self-similar

chains of metal nanoparticles,[12,13] nanostars,[14] nanocresents,[15,16] and nanogratings,[17,18] where the energy splitting of LSP resonant modes may be achieved by an inappreciable change of, e.g., the nanogap size in the nanostructures, which leads to a pronounced shift of resonant frequencies. Therefore, the fine control of nanogaps[19,20] or nanotips[21] in such structures is crucial for generating, sustaining, and steering strong LSPs.

Field enhancement by orders of magnitude in the nanogaps of plasmonic nanostructures has been demonstrated and has been applied in, for example, material analysis,[17,18] optical rectification,[19] optical near-field characterization,[21] sensing,[22] nonlinear optics,[23] and high-sensitivity plasmonic rulers.[24] Stockman and co-authors[4] proposed a cascaded self-similar nanoantenna chain that can significantly boost the enhancement–localization ratio of the LSPs. Cascaded field enhancement was achieved by using coupled gold nano-antennae of decreasing sizes. V-shaped nanogrooves and waveguides, another type of nanostructure with tiny gaps, are often used as light-concentration device,[25–27] in which the field can be strongly confined in the bottom of the V gaps and the EM energy can be transferred between the LSPs and the propagating SP waves. Based on these heuristic ideas and structures, several research groups[2,4,6,12,13] have proposed many useful functional applications of V nanogrooves.

In the practical application of such plasmonic nanostructures, the key issues are the precise control of the nanogaps and the uniformity of the whole structure, which gives much challenge to nanofabrication.[28–30] In previous works,[28–30] metallic nanostructures separated by tiny gaps were usually fabricated by using electron-beam lithography (EBL), which has a relatively low yield and high cost. Nanoimprinting lithography (NIL)[29] is well known to be able to replicate nanostructures in a large area with relatively low cost, but for nanostructures with tiny gaps, the mother stamp for imprinting is difficult to fabricate. Nanosphere lithography[31–33] is also a possible choice, but it is difficult to finely control and tune the nanogap size with this technique. With all these methods it is still challenging to achieve high-quality plasmonic nanostructures with both nanogaps and uniform large area. Therefore, a reliable and cost effective nanofabrication method is highly demanded in this regard.

Herein, we propose a simple M-shaped plasmonic nanograting structure, in which V-shaped nanogrooves with tens of nanometer width for sustaining strong LSPs can be readily realized uniformly in a large area. We develop a reliable technique based on room-temperature nanoimprinting lithography (RT-NIL)[34–36] and anisotropic reactive-ion etching (RIE) to fabricate this structure. The EM field localization and enhancement in the V grooves of the M grating are analyzed by rigorous numerical simulation and are experimentally characterized by scanning near-field optical microscopy (SNOM). Finally, to demonstrate the potential application of this plasmonic nanostructure with tiny nanogaps, we employ the M grating as a substrate for surface-enhanced Raman spectroscopic (SERS) sensing. By probing Rhodamine 6G (R6G) molecules experimentally, the SERS enhancement factor is evaluated, and the existence of strongly localized field hot spots and the enhanced light–matter interaction in the substrate structure is verified.

2. Methods

2.1. The M-Grating Design

The M grating is designed to have an M-shaped profile so that it can generate relatively deep V grooves that have a width of only tens of nanometers between adjacent M shapes, by taking into account the anisotropic RIE fabrication process (see details in the Experimental Section). The schematic geometry of the M-grating is shown in **Figure 1**A; it has a period d, groove heights h_1 and h_2, nanogap width w, and geometrical vertex angles θ_1 and θ_2. θ_2 is crucial as it determines the size of the nanogap and should be controlled carefully in the nanofabrication process. A gold film of thickness $t =$ 30 nm is coated on the grating surface by using vacuum deposition. As a consequence of this deposition method, the film on the side wall of the M profile is usually thinner than that on the top surface (as shown in Figure 1A). In our numerical simulations, the refractive index of gold was taken from a dispersion model based on experimental data.[37,38]

In the design of the gold-film-coated M-grating, it is crucial to have tiny gaps (with $w \approx$ tens of nanometers) between the adjacent M shapes to generate a strongly enhanced localized field inside the narrow V grooves with θ_2 apex. We used the commercial software COMSOL 4.3®, which is based on the finite-element method, to rigorously simulate the field distribution in the M grating. The grating is illuminated by a plane wave whose incident plane is perpendicular to the grating lines. Then both the structure and the incident light field are invariant along the z axis (see Figure 1A), which can be treated as a two-dimensional problem in the simulation. The polarization of the incident field is denoted as TM (TE), if its magnetic (electric) field component is perpendicular to the incident plane. To excite LSPs effectively in the grating, the incident polarization is usually chosen as TM.

Without the loss of generality, we designed an M grating under the normal incidence of a TM polarized plane wave with wavelength $\lambda =$ 785 nm (which is a commonly used excitation wavelength in Raman spectroscopy). To get the most reliable simulation results, we created the grating geometry as close as possible to the practically fabricated samples, by rounding each sharp corner of the M profile by a radius of curvature of 10 nm (as shown in Figure 1A, and also see detailed discussion on the influence of curvature radius on the field localization in Section 1 of the Supporting Information). The electric-field amplitude of the incident light was normalized as $|\mathbf{E}_0| = 1$, so that the field enhancement factor can be evaluated directly by the amplitude of the excited-field distribution in the M grating as $|\mathbf{E}/\mathbf{E}_0| = |\mathbf{E}|$.

To produce pronounced LSP resonance at 785 nm, we have made a thorough numerical study of the field distribution in the M grating with respect to the change of nanogap size w. When w is around 30 nm, the best field localization and enhancement results can be obtained, as shown in Figure 1B. To generate this size of nanogaps by using the
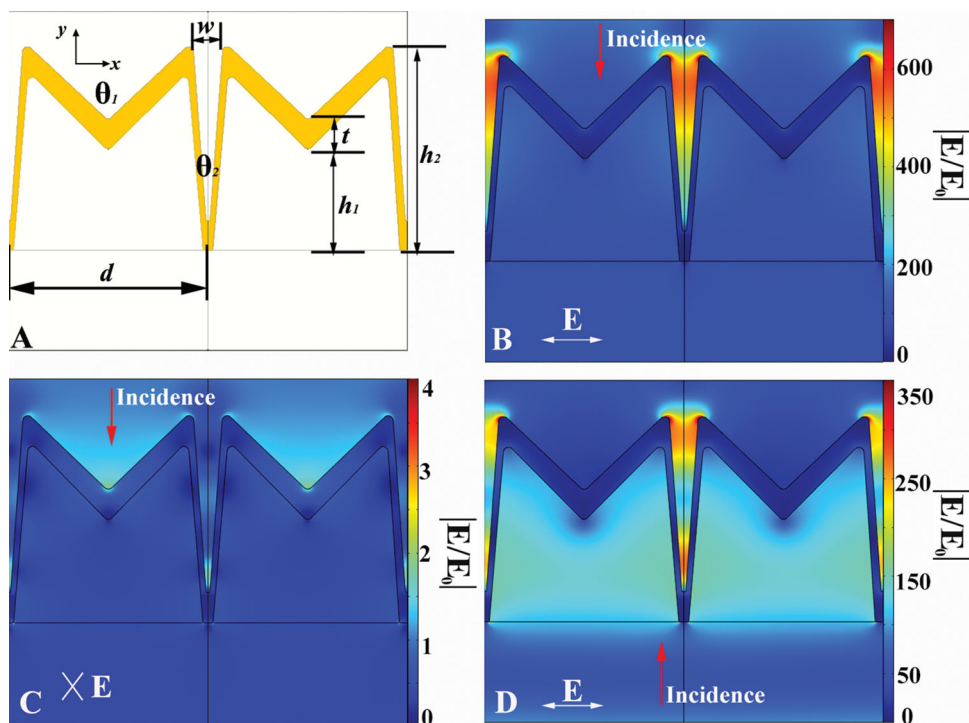
Figure 1. A) Schematic geometry of the M grating. B) and C) are the numerical simulation results of the electric field amplitude distribution in a M grating with $d = 200$ nm, $h_1 = 120$ nm, $h_2 = 180$ nm, $\theta_1 = 85°$, and $\theta_2 = 10°$, under the normal incidence of a TM or TE polarized-plane wave with wavelength 785 nm from the top side, respectively. D) is the same as B), but under the normal incidence of a TM polarized-plane wave with wavelength 633 nm from the back side.

anisotropic RIE process (as explained in Section 2.2 and the Experimental Section), the period of the grating was chosen as $d = 200$ nm, which is one of the most crucial parameters for fabrication. The other geometrical parameters were: $h_1 = 120$ nm, $h_2 = 180$ nm, $\theta_1 = 85°$, and $\theta_2 = 10°$.

Figure 1B shows the simulated electric field distribution in this M grating under the normal incidence of TM-polarized light from the top side, where we can evidently see the pronounced field localization and enhancement (with an enhancement factor up to 700) in the whole open area of the V groove. This field localization and enhancement is generated by the efficient coupling of the LSPs confined on the two adjacent corners of the M-grating profile due to their small spacing separated by the V groove. This is the same principle as the LSP coupling reported in many previous works,[4,7,13,16,20] in which the enhanced field is generated in the tiny gaps between metallic nanoparticles due to their strong intercoupling with decreased spacing. This gap effect[2] is of central importance to the performance of many plasmonic nanosensors. To validate this LSP coupling mechanism, we calculated the field distribution in the same M grating under TE illumination (as shown in Figure 1C). Obviously, there is almost no field localization and enhancement on the M-grating surface (where the maximum field enhancement factor is no more than 2), because in this polarization mode the LSPs cannot be effectively excited. Furthermore, since the LSP oscillations are along the grating lines in this case, there is also no effective coupling between the hot spots on the adjacent corners of the V groove.

The above calculations show that the coupling of the LSPs on the two corners of the narrow V groove is the main cause of field localization and enhancement in the nanogap. However, the field localization in the wider groove with apex angle θ_1 may also contribute to the coupling, because the two grooves are so close to each other. To validate this, we have simulated four different grating structures as shown in **Figure 2**. In Figures 2A and 2B, we consider a grating with only the wide groove with apex $\theta_1 = 85°$ or only the narrow groove with apex $\theta_2 = 10°$, respectively. Clearly, the field can be localized and enhanced in both grooves, but the field enhancement factor depends on the vertex angle and depth of the groove significantly: with narrower and deeper grooves, the field is confined better and enhanced more significantly, even though the field enhancement factor in both structures (the maximum is about 70 in Figure 2B and 4 in Figure 2A) is much smaller than that in the M grating in Figure 1B. On the other hand, in the deeper and narrower grooves in Figure 2B, the LSPs exhibit a higher order cavity mode,[8,39,40] unlike that in the M grating. All these results imply that the remarkable field enhancement in the nanogap of M grating stems from the strong coupling of the LSP states supported by the two individual V grooves, as presented in Figures 2A and 2B. Owing to the polarization and momentum matching under TM illumination, the dipolar oscillations of the LSPs in the two grooves can couple with each other strongly. In other words, the LSPs in the shallow groove can modulate the LSPs in the deep groove. Consequently, a new LSP resonance mode is generated in the M grating (as shown in Figure 1B)
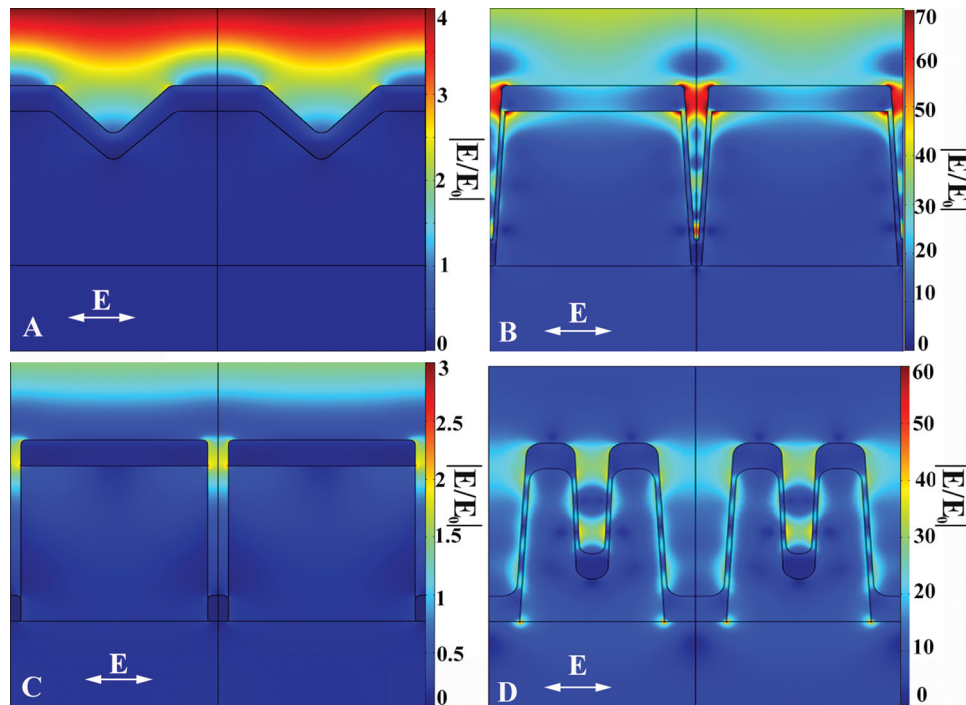
Figure 2. Simulated electric-field distributions: A) A grating with only the wide V groove with vertex angle $\theta_1 = 85°$, B) a grating with only the narrow V groove with vertex angle $\theta_2 = 10°$, C) a grating with rectangular nanogaps of 30-nm width, and D) a grating (named the M1 grating) with two rectangular nanogaps of widths 60 nm and 30 nm. All calculations were performed under normal incidence of a TM-polarized-plane wave with wavelength 785 nm from the top side.

which is significantly different from the LSP mode in each individual V groove.

To better understand this coupling mechanism, we also simulated two additional grating structures under the same incidence condition as the M grating (TM polarization, normal incidence, $\lambda = 785$ nm), as shown in Figures 2C and 2D. Figure 2C is a rectangular nanograting with $d = 200$ nm, groove depth $h = 180$ nm, gold film (only on top of the grating ridge and at the bottom of the groove) thickness $t = 30$ nm, and a 30-nm-wide rectangular nanogap. Clearly, there is almost no field localization and enhancement in the whole structure (where the maximum field enhancement factor is no more than 2). In this case, there is only one nanogap in one period so that no intercoupling between nanogaps can be generated; on the other hand, the rectangular nanogap shows much weaker field confinement than the V groove.

Figure 2D shows another type of M-shaped nanograting (named M1 grating hereafter), of which the profile is fitted according to one of our fabricated samples. The main grating parameters such as the period and the gold film thickness are the same as those of the M grating in Figure 1, but the grating profile is modified so that the nanogaps are almost rectangular instead of V shaped. The widths of the two nanogaps in a period are 30 nm and 60 nm, and the heights are $h_1 = 50$ nm and $h_2 = 180$ nm. The simulation results show that the EM field can still be localized in the nanogaps, but the intensity of the localized field is much weaker than in Figure 1B. The maximum field enhancement factors in the narrower gap and in the wider groove are about only 40 and 25, respectively. This result shows again that the field localization in the rectangular nanogap is much weaker than that in the V groove

and the intercoupling of the LSPs in the two rectangular nanogaps is also much weaker.

According to the above analyses, we may conclude that the strong field localization in the narrow V-shaped nanogap and the intercoupling of LSPs in the two adjacent grooves are the key factors to generate the strongly localized and enhanced EM field. The intercoupling is strongly dependent not only on the nanogap size but also on its shape, so that the V-shaped grooves (in Figure 1B) behave better than the rectangular grooves (in Figure 2D). Therefore, fine control of the V-shaped nanogaps is crucial for generating and sustaining an enhanced localized EM field.

2.2. Fabrication of the M Grating

We have developed a RT-NIL technique to fabricate the M grating. The whole fabrication process is sketched in **Figure 3**A. Firstly, two layers of photoresists, including a 350-nm-thick polymethylmethacrylate (PMMA) bottom layer and a 200-nm-thick hydrogen silsequioxane (HSQ) top layer, were spin-coated sequentially onto a cleaned gallium nitride (GaN) substrate. Then, the RT-NIL process was operated by using a rectangular nanograting stamp with period 100 nm, grating line-width 50 nm, and groove depth 250 nm, which was fabricated by standard EBL on a quartz substrate. After demolding, an RIE process was performed with pure CF_4 to remove the residual HSQ in the imprinted grooves. Then, with the HSQ mask, the PMMA layer was etched through by RIE with pure O_2 plasma. Afterwards, with the nanostructured HSQ/PMMA bilayer mask, another anisotropic RIE
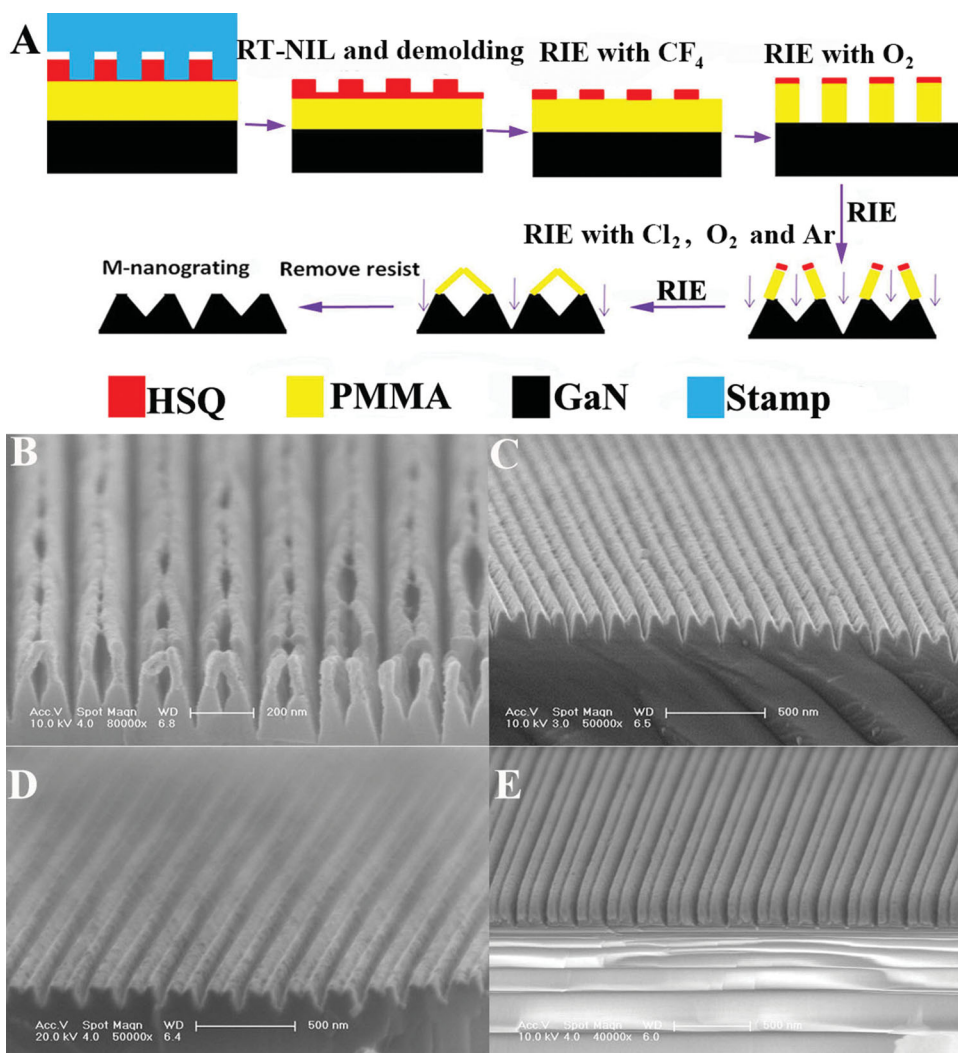
Figure 3. A) Schematic of the fabrication process of the M grating, which combines RT-NIL and anisotropic RIE. B–E) cross-sectional SEM images of four samples. B) and C) show the M grating before and after removing the HSQ/PMMA photoresist bilayer after the RIE. D) M grating after a 30-nm-thick gold layer was coated onto it. E) Profile of a fabricated M1 grating coated with a 30-nm-thick gold layer.

process was employed to etch the underneath GaN substrate in O_2 10/Ar 10/Cl_2 48/CF_4 26 sccm plasma; this is the crucial process to form the M-grating profile. Finally, after removing the residual resists by bathing the structured samples in acetone, a desired thickness of metal film (e.g., a 30-nm thick gold film as we used here) was deposited onto the surface of the nanostructure to achieve the M grating.

In the above procedure, the formation of the M-shaped profile is crucial; this is controlled by anisotropic RIE. In this process, since the HSQ layer was cured gradually from the top down by O_2 plasma, the PMMA layer received a lateral etching during the Ar plasma blasting to form the raster gate lines on the GaN substrate. At about the halfway point of the etching process, each two adjacent PMMA raster gate lines collapsed into each other because they could no longer hold under the Ar and O_2 plasma bombing; the collapse direction was predominantly determined by the interface tension of the polymeric raster gate lines. The gradual collapse procedure was determined by the power and operating time of O_2 and Ar plasma bombing. During this process, the GaN substrate was etched nonuniformly: in the area covered by the collapsed line pairs, the etching speed was relatively slower; while in the area outside the collapsed line pairs, the etching speed was faster. After the line pairs completely collapsed into each other, the etching was stopped in the regions underneath the photoresist line pairs. However, the etching of the uncovered regions continued until the operating time was over. In this way, a nanograting with an M-shaped profile was gradually formed.

The structure parameters of the fabricated samples were measured from the scanning electronic microscope (SEM, FEI Serion2000) images of the M grating before and after the gold-film coating (as shown in Figures 3C and 3D, respectively). They are very close to the designed parameters. Figure 3B shows the SEM image of an M-grating sample right after the anisotropic RIE etching and before the removal of the bilayer resist, which verifies the etching mechanism stated above. The V-groove angles can be controlled by tuning the dry-etching parameters. For example, by changing the etching recipe to Ar 5/Cl_2 48/CF_4 10 sccm, we can obtain
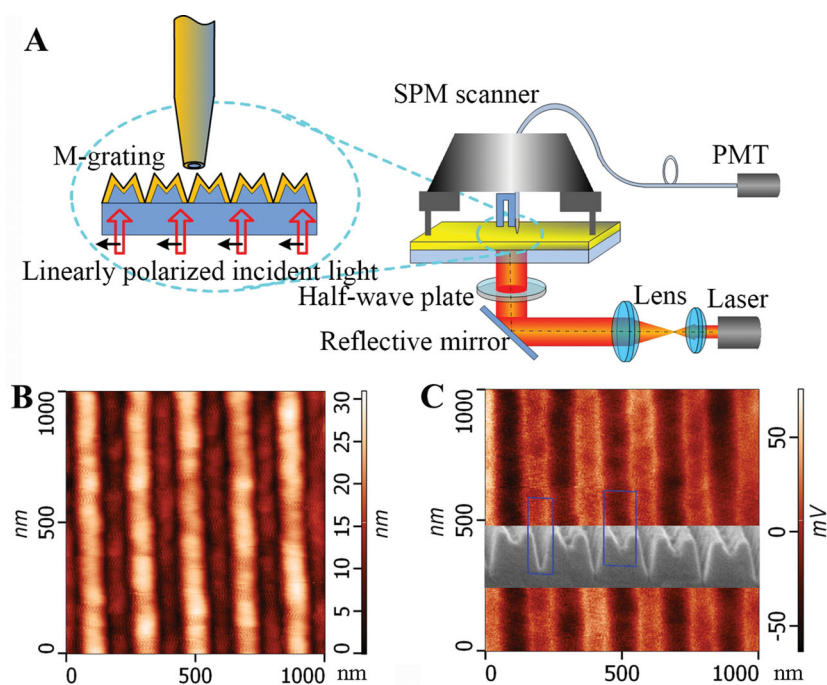
Figure 4. A) Schematic of the transmission-type SNOM. B) The measured topography of the M-grating sample, where the color corresponds to the height of the profile. C) The measured optical near-field intensity mapping on the M-grating sample surface. The color shows the PMT signal intensity. The inset is an SEM image of the M-grating cross-section corresponding to the field map.

an M1-grating profile (as shown in Figure 3E), where the nanogap widths are 30 nm and 60 nm and the groove heights are $h_1 = 50$ nm and $h_2 = 180$ nm (corresponding to the simulated structure in Figure 2D). A detailed discussion on profile control to generate M or M1 grating is presented in Section 3 of the Supporting Information.

The proposed method is suitable for fabricating large-area M-grating substrates while maintaining relatively good uniformity. In our experiment, the fabricated sample has an operating area as large as 10 cm², as shown in Figure S2. A detailed discussion on the fabrication of large-area and uniform SERS substrates is given in Section 2 of the Supporting Information.

3. Experimental Study of the Field Enhancement in the M Grating

3.1. Near-Field Characterization

To investigate the field localization and enhancement in the M grating experimentally, a SNOM (NT-MDT NTEGRA, Russia) equipped with an aperture optical fiber probe was used to spatially map the near-field distribution on the surface of the M grating. **Figure 4**A shows a schematic of the transmission-type SNOM setup. The M-grating sample, which was mounted on a piezo-scanner table, was illuminated normally by using a collimated He–Ne laser beam of 633-nm wavelength from the back side. At normal incidence we had to illuminate the sample from the back side (not the top side) to avoid mechanical interference between the incident

light beam and the fiber probe; a 633 nm laser (instead of a 785 nm one) was used as the light source to illuminate the sample because the light is visible and can facilitate the adjustment of the optical setup. Due to these differences from our theoretical simulation, we should re-evaluate the field localization in the M grating in this case. The simulated field distribution in the same M grating as in Figure 1B but under the normal illumination of a TM-polarized plane wave of 633-nm wavelength from the back side is shown in Figure 1D. The field distribution in general is similar to that in Figure 1B, except that the field intensity is weaker (with an enhancement factor up to 350) and a higher order cavity mode appears in the V groove. This result is because the LSP resonance usually exists in a relatively broad wavelength range, so that similar field localization and enhancement effect can still be observed at 633-nm wavelength. Since the field distributions at these two wavelengths are greatly similar and only a little different in strength, we can use the 633-nm laser to characterize the field localization in the M grating.

An aperture fiber probe was located on the opposite side of the sample to collect the near-field signal (as shown in Figure 4A). The field on the M-grating surface was measured by a photomultiplier tube (PMT). The intensity distribution of the near-field optical signal was mapped by scanning the probe tip over the central region of the M grating. By using this technique, the topography of the grating sample and the near-field distribution image can be obtained simultaneously, as shown in Figures 4B and 4C, respectively. Due to the limited spatial resolution of the SNOM probe, the topography in Figure 4B does not show much detail of the M profile. However, the positions of the grating ridges and grooves (bright and dark regions in Figure 4B, respectively) are clearly demonstrated. The correspondence between the topography of the M-grating profile and the near-field distribution on the grating surface is clearly seen by comparing Figures 4B and 4C. As indicated by the blue boxes in Figure 4C, the EM field is mainly localized in the open area of the narrow V groove and is greatly enhanced therein (see the bright regions, where the PMT signal intensity is up to 50 mV). Moreover, the field on the two edges of the narrow V groove is stronger than that in the middle of the V groove. All these features correspond well with the numerical simulations in Figure 1B. Therefore, it is experimentally verified that strong field localization and enhancement can exist in the V-shaped nanogaps of the M grating, as predicted by the numerical simulations.

3.2. SERS Experiment

As a demonstration of the potential application of the proposed M grating, the sample was used as a SERS substrate
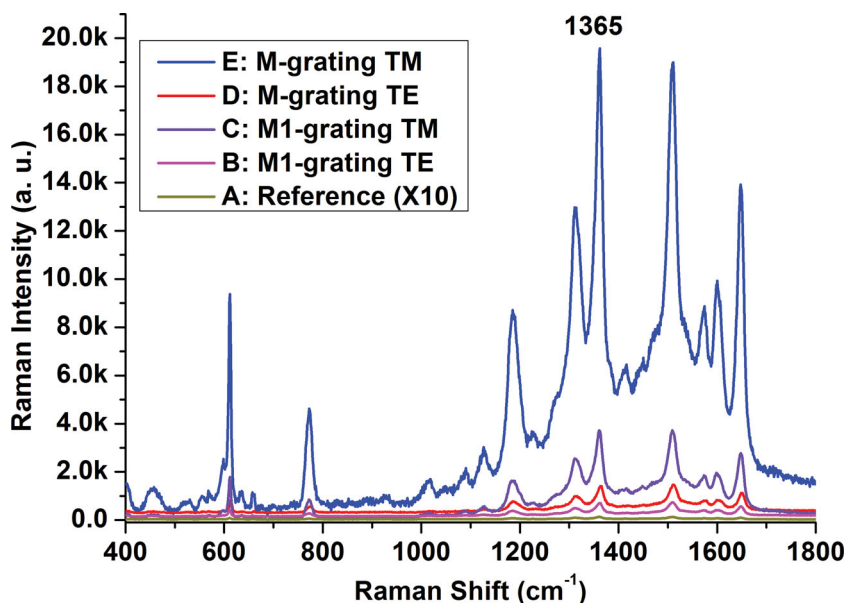
Figure 5. Measured Raman spectra of the R6G molecules on different substrates. A) The reference Raman spectrum collected from the unpatterned gold film. B) and C) are the SERS spectra measured on the M1 grating under TE and TM illuminations, respectively. D) and E) are the same as B) and C), but for the M grating. The 1365 cm^{-1} band is the characteristic vibration wavenumber of the R6G molecules.

enhanced localized field and light–matter interaction on the M-grating surface.

To quantitatively evaluate the SERS performance of the M-grating substrate, we calculated the SERS enhancement factor (EF) of the probing R6G molecules using Equation 1:[28]

$$EF = \frac{I_{SERS}/N_{surf}}{I_{bulk}/N_{bulk}} \qquad (1)$$

where I_{SERS} and I_{bulk} are the Raman signal intensities at 1365 cm^{-1} (which is a characteristic vibration wavenumber of R6G molecules) detected from the R6G molecules adsorbed on the grating surface and from bulk R6G molecules, respectively, and N_{surf} and N_{bulk} are the estimated numbers of R6G molecules absorbed on the grating surface and bulk R6G molecules exposed to the laser spot, respectively. We estimated the number of R6G molecules doped per unit period N_{surf} to be 2×10^2. Thus, according to Equation (1), the SERS EF of the M grating under TM illumination can be estimated to be as high as 5×10^8. This experimental EF value is comparable with but a little smaller than the theoretically estimated EF, which is calculated to be EF $\approx |E|^4 = |E/E_0|^4 \approx 10^{10}$.[2] The difference can be attributed to the experimental errors and theoretical estimation errors. In contrast, the experimental EF value of the M1 grating is only 5×10^3.

Furthermore, it is meaningful to evaluate the SERS sensitivity of the M-grating substrate. For this aim, we have experimentally investigated the detection limit of the R6G molecules (see details in Section 4 in the Supporting Information). By measuring R6G solutions of various concentrations, the lowest concentration of R6G solution that can produce effective Raman signal from the M-grating substrate was determined as 0.02 μm, which can act as a gauge of the SERS sensitivity of the device.

These SERS experiments provide concrete evidence that the M grating has much better SERS performance than the reference M1 grating, owing to the much stronger field localization and significant enhancement in the V-shaped nanogaps. Therefore, the M grating has great potential to be used as a low-cost, replicable, high-performance active substrate for SERS applications.

for probing R6G molecules (bulk concentration=0.1 μm). The R6G molecules were dosed onto the M-grating surface. The back-scattered Raman spectra were recorded by using a LabRam microRaman system (Jobin-Yvon/ISA HR) equipped with a thermoelectrically cooled charge-coupled device (CCD) array detector and an Olympus BH-2 100× short-focal-length objective lens (nominal numerical aperture=0.85). A continuous-wave GaAs laser (Spectra Physics 3900s) of 785-nm wavelength and output power of 0.6 mW was used to excite the samples.

The SERS spectra of the R6G molecules were collected in the Raman shift range of 200–2000 cm^{-1}, in one acquisition and in an accumulation time of 10 s. The reference spectrum was collected from the unpatterned area (i.e., a flat surface with gold film only) on the same device, in five acquisitions and with the accumulation time of 10 s. All the data were fitted from the baseline-removed Raman spectra using a Gaussian–Lorentzian line shape. **Figure 5** shows the detected SERS spectra of the R6G molecules on the M-grating and M1-grating substrates, as well as the reference spectrum on a flat gold surface.

In Figure 5, the SERS signal collected from the M-grating sample under TM illumination (i.e., curve E) is the strongest, much stronger than not only the reference spectrum collected from the naked gold film but also the spectra collected from the M1 grating under both TE and TM illumination and the M grating under TE illumination. Since the experiment conditions are the same for all the samples, the SERS enhancement can be solely attributed to the field enhancement on the surfaces of the plasmonic nanostructures. These SERS experimental results are consistent with the simulated field enhancement factors on the surfaces of the structures (as seen in Figures 1B, 1C, and 2D), verifying the greatly

4. Conclusion

We have proposed and presented the design and fabrication of a simple M-shaped nanograting with tiny gaps of tens of nanometers. Mediated by the localization and intercoupling of LSPs, strong field amplitude enhancement up to 700-fold can be generated in the opening area of the narrow V grooves, thanks to the special M-shaped profile. A nanofabrication technique based on RT-NIL and anisotropic RIE has

been developed to fabricate this novel plasmonic device with well-controlled nanogap size and shape, which is cost effective, reliable, and suitable for fabricating large-area nanostructures. The field localization and coupling mechanisms were analyzed theoretically by using numerical simulation and characterized experimentally by using SNOM measurements. This M-grating device has excellent prospects in many plasmonic applications such as ultrasensitive sensing of chemical and biological substances. As a demonstration of the potential application, the M grating was used as a SERS substrate for probing R6G molecules. Experimentally, an average SERS enhancement factor as high as 5×10^8 was achieved, verifying the greatly enhanced light–matter interaction on the surface of the M grating.

5. Experimental Section

M Grating Fabrication: A quartz stamp patterned with linear rectangular grating with period of 100 nm and duty cycle of 0.5 was fabricated by using EBL. Then the nanoimprinting resists HSQ (XR-1541–006, Dow Corning, USA) and PMMA (MicroChem, PMM A950A4) were spin-coated onto the GaN substrate to the appropriate thickness (determined by mold depth, duty cycle, and period), baked on a hotplate (70 °C, 5 min) to remove residual solvent, and imprinted with a custom-built nanoimprinter (50 psi, 5 min, at room temperature). After separation of the mold and substrate, the residual HSQ was removed in CF_4 plasma (40 sccm, 2 Pa, 40 W, 10 s) and the bottom PMMA layer was etched with O_2 plasma (48 sccm, 26 Pa, 70 W, 30 s). The pattern was transferred into the GaN substrate by using RIE (M grating: 48/26/10/10 sccm $Cl_2/CF_4/O_2/Ar$, 100 W, 16 Pa, 2 min; M1 grating: 48/10/5 sccm $Cl_2/CF_4/Ar$, 40 W, 26 Pa, 2 min). The final resist was removed by soaking in acetone and using a low-power ultrasonic bath, rinsed with methanol and isopropanol (IPA), and dried using a steady stream of N_2.

Metal Deposition: Metal deposition was performed by using an electron beam evaporator (L-400EK Evaporation System, ANELVA, Japan). A 30-nm-thick gold film was deposited onto the sample at the operating pressure of 5×10^{-5} Pa. The temperature of the sample chamber was kept at 20 °C during the entire evaporation process, with the sample holder rotating at a rate of 40 rmp to ensure the uniformity of deposition. A general adhesive layer such as Cr or Ti was not necessary.

Numerical Simulation: Numerical simulations were performed on a workstation by using the commercial software COMSOL 4.3® based on the finite-element method. To obtain a EM field distribution as close as possible to the practical situation, we defined the M profile by rounding each sharp corner by a radius of curvature of 10 nm. Periodic boundary condition was used in the *x* direction to simulate an infinite array of periodic M grating. Perfectly matched layer boundary conditions were executed in the *y* direction. The mesh size used in the simulation regions was 1 nm. The gratings were illuminated by a plane wave propagating along the *y* direction. The total electric field amplitude was calculated to generate the field distribution in the structures. The refractive indices of gold and GaN were taken from a dispersion model based on experimental data and the Palik database, respectively.[37,38]

Instrumentation: SEM (FEI Serion200) and AFM (NT-MDT NTEGRA, Russia) in tapping mode was used to measure the morphology of samples. The Raman spectra were recorded using a LabRam microRaman system (Jobin-Yvon/ISA HR) with a 785 nm GaAs laser source at room temperature and configured with a CCD array detector and an Olympus BH-2 100× short focal length objective lens (nominal numerical aperture is 0.85). The Raman signal probing area was about 3 µm in diameter. The incident power at the sample surface was 0.6 mW with an integration time of 10 s.

Surface-Enhanced Raman Scattering: To evaluate the SERS performance of the M-grating samples, a R6G (Sigma-Aldrich Co.) aqueous solution (with a concentration of 0.1 µm) was used. To allow molecule adsorption, the substrates were maintained for 12 h in the R6G solution, and then taken out and rinsed several times with IPA. The rinsing process ensured the formation of approximate a monolayer of R6G molecules over the surface of gold film. The acquisition time and laser power were the same for all Raman spectra. The SERS spectra were recoded from multiple sites on the substrate surface to confirm reproducibility. Similar SERS spectra characteristics, such as enhancement, position, and relative intensity of the bands, were determined from various locations due to the large-area production of the uniform geometries. The signal of reference was collected from the unpatterned regions of the same substrate. Since the concentration of R6G molecules in the detection regions was the same on both the patterned and unpatterned regions, the enhanced Raman scattering can be attributed solely to the field enhancement caused by the nanostructures. So the chemical factor for Raman-scattering enhancement is ignored.

[1] W. L. Barnes, A. Dereux, T. W. Ebbesen, *Nature* **2003**, *424*, 824.

[2] M. I. Stockman, *Opt. Express* **2011**, *19*, 22029–22106.

[3] J. A. Schuller, E. S. Barnard, W. Cai, Y. C. Jun, J. S. White, *Nat. Mater.* **2010**, *9*, 193.

[4] M. I. Stockman, S. V. Faleev, D. J. Bergman, *Phys. Rev. Lett.* **2002**, *88*, 067402.

[5] J. A. Dionne, L. A. Sweatlock, H. A. Atwater, A. Polman, *Phys. Rev. B* **2006**, *73*, 035407.

[6] K. Li, M. I. Stockman, D. J. Bergman, *Phys. Rev. Lett.* **2003**, *91*, 227402.

[7] T. Shegai, Z. Li, T. Dadosh, Z. Zhang, H. Xu, G. Haran, *Proc. Nat. Acad. Sci. USA* **2008**, *105*, 16448.

[8] R. Ameling, H. Giessen, *Laser Photonics Rev.* **2013**, *7*, 141.

[9] N. J. Halas, *Proc. Nat. Acad. Sci. USA* **2009**, *106*, 3643.

[10] M. Moskovits, *Phys. Chem. Chem. Phys.* **2013**, *15*, 5301.

[11] E. Prodan, C. Radloff, N. J. Halas, P. Nordlander, *Science* **2003**, *302*, 419.

[12] B. Ding, Z. Deng, H. Yan, S. Cabrini, R. N. Zuckermann, J. Bokor, *J. Am. Chem. Soc.* **2010**, *132*, 3248.

[13] C. Hoppener, Z. J. Lapin, P. Bharadwaj, L. Novotny, *Phys. Rev. Lett.* **2012**, *109*, 017402.

[14] F. Hao, C. L. Neh, J. H. Hafner, P. Nordlander, *Nano Lett.* **2007**, *7*, 729.

[15] A. I. F. Domínguez, Y. Luo, A. Wiener, J. B. Pendry, S. A. Maier, *Nano Lett.* **2012**, *12*, 5946.

[16] S. Cataldo, J. Zhao, F. Neubrech, B. Frank, C. Zhang, P. V. Braun, H. Giessen, *ACS Nano* **2012**, *6*, 979.

[17] X. Deng, G. B. Braun, S. Liu, P. F. Sciortino, B. Koefer, T. Tombler, M. Moskovits, *Nano Lett.* **2010**, *10*, 1780.

[18] W.-D Li, F. Ding, J. Hu, S. Y. Chou, *Opt. Express* **2011**, *19*, 3925.

[19] D. R. Ward, H. Falco, F. Pauly, J. C. Cuevas, D. Natelson, *Nat. Nanotechnol.* **2010**, *5*, 732.

[20] H. Duan, A. I. F. Domínguez, M. Bosman, S. A. Maier, J. K. W. Yang, *Nano Lett.* **2012**, *12*, 1683.

[21] F. Huth, A. Govyadinov, S. Amarie, W. Nuansing, F. Keilmann, R. Hillenbrand, *Nano Lett.* **2012**, *12*, 3973.

[22] N. Liu, M. L. Tang, M Hentschel, H. Giessen, A. P. Alivisatos, *Nat. Mater.* **2011**, *10*, 631.

[23] P. Genevet, J. Tetienne, E. Gatzogiannis, R. Blanchard, M. A. Kats, M. O. Scully, F. Capasso, *Nano Lett.* **2010**, *10*, 4880.

[24] N. Liu, M. Hentsche, T. Weiss, A. P. Alivisatos, H. Giessen, *Science* **2011**, *332*, 1407.

[25] M. Schnell, P. Alonso-Gonzalez, L. Arzubiaga, F. Casanova, L. E. Hueso, A. Chuvilin, R. Hillenbrand, *Nat. Photonics* **2011**, *5*, 283.

[26] C. L. C. Smith, B. Desiatov, I. Goykmann, F. Irene, U. Levy, A. Kristensen, *Opt. Express* **2012**, *20*, 5696.

[27] H. Gao, J. Henzie, M. H. Leeb, T. W. Odom, *Proc. Nat. Acad. Sci. USA* **2008**, *105*, 20146.

[28] H. Duan, H. Hu, K. Kumar, Z. Shen, J. K. W. Yang, *ACS Nano* **2011**, *5*, 7593.

[29] S. Y. Chou, Q. Xia, *Nat. Nanotechnol.* **2008**, *3*, 295.

[30] J. Henzie, J. Lee, M. H. Lee, W. Hasan, T. W. Odom, *Annu. Rev. Phys. Chem.* **2009**, *60*, 147.

[31] W. A. Murray, W. L. Barnes, *Adv. Mater.* **2007**, *19*, 3771.

[32] X. Zhang, M. A. Young, O. Lyandres, R. P. Van Duyne, *J. Am. Chem. Soc.* **2005**, *127*, 4484.

[33] Y. Fang, N.-H. Seong, D. D. Dlott, *Science* **2008**, *321*, 388.

[34] K. Nakamatsu, K. Watanabe, K. Tone, T. Katase, W. Hattori, Y. Ochiai, T. Matsuo, M. Sasago, H. Namatsu, M. Komuro, S. Matsui, *Japan. J. Appl. Phys.* **2004**, *43*, 4050.

[35] Z. Zhu, Q. Li, L. Zhang, M. Chen, S. S. Fan, *J. Vac. Sci. Technol. B* **2011**, *29*, 021015.

[36] H. Zhang, J. Zhu, Z. D. Zhu, G. F. Jin, *Opt. Express* **2013**, *21*, 13492.

[37] M. L. Theye, *Phys. Rev. B* **1970**, *2*, 3060.

[38] P. B. Johnson, R. W. Christy, *Phys. Rev. B* **1972**, *6*, 4370.

[39] P. Genevet, J.-P. Tetienne, E. Gatzogiannis, E. Gatzogiannis, R. Blanchard, M. A. Kats, M. O. Scully, F. Capasso, *Nano Lett.* **2010**, *10*, 4880.

[40] R. Ameling, D. Dregely, H. Giessen, *Opt. Lett.* **2011**, *36*, 2218.